RSC Advances

PAPER

View Article Online
View Journal | View Issue

Cite this: *RSC Adv.*, 2016, **6**, 85457

Shear stress magnitude and transforming growth factor-βeta 1 regulate endothelial to mesenchymal transformation in a three-dimensional culture microfluidic device†

Sara G. Mina,[a] Wei Wang,‡[b] Qingfeng Cao,[b] Peter Huang,[b] Bruce T. Murray[b] and Gretchen J. Mahler*[a]

Normal fibroblasts are present within the extracellular matrix (ECM). They can become activated, leading to increased proliferation and ECM protein secretion such as collagen type I to promote tissue remodeling. These cells are also involved in adult pathologies including cancer metastasis and cardiac and renal fibrosis. One source of activated fibroblasts is endothelial to mesenchymal transformation (EndMT), in which endothelial cells lose their cell–cell and cell–ECM adhesions, gain invasive properties, and become mesenchymal cells. While EndMT is well characterized in developmental biology, the mechanisms and functional role of EndMT in adult physiology and pathology have not been fully investigated. A microfluidic device with an incorporated three-dimensional ECM chamber was developed to study the role of combined steady fluid shear stress magnitudes and transforming growth factor-βeta 1 (TGF-β1) on EndMT. Low (1 dyne per cm^2) steady shear stress and TGF-β1 exposure induced EndMT in endothelial cells, including upregulation of mesenchymal protein and gene expression markers. Cells exposed to TGF-β1 and high (20 dynes per cm^2) steady shear stress did not undergo EndMT, and protein and gene expression of mesenchymal markers was significantly downregulated. Mesenchymally transformed cells under static conditions with and without TGF-β1 showed significantly more collagen production when compared to fluidic conditions. These results confirm that both low shear stress and TGF-β1 induce EndMT in endothelial cells, but this process can be prevented by exposure to physiologically relevant high shear stress. These results also show conditions most likely to cause tissue pathology.

Received 27th June 2016
Accepted 30th August 2016

DOI: 10.1039/c6ra16607e

www.rsc.org/advances

Introduction

Endothelial to mesenchymal transformation (EndMT) is a physiological cellular response involved in embryonic heart valve development.[1] However, recent studies have shown that mesenchymal transformation can also occur in tissue homeostasis, such as wound healing, and in adult pathologies, including cancer, atherosclerosis, cardiac and renal fibrosis, and calcific aortic valve disease.[1,2] EndMT begins when vascular or valvular endothelial cells delaminate from their cell monolayer, and lose cell–cell contacts and endothelial markers such as vascular endothelial cadherin (VE-cadherin). These cells gain mesenchymal or fibroblast-like markers such as alpha-smooth muscle actin (α-SMA), and acquire mesenchymal cell-like properties.[3–5] Cell transformation from endothelial to mesenchymal phenotype is followed by cell invasion into and remodeling of the extracellular matrix (ECM). This transformation has been found to be responsible for generating cancer activated fibroblasts (CAFs) in transgenic tumor grown mice.[3] These CAFs remodel the ECM and secrete biochemical signaling factors that affect the behavior of cells within the tumor microenvironment leading to metastasis.[6] Two stimuli that have been shown to induce EndMT are changes in hemodynamic forces (such as fluid shear stress)[7] and increased exposure of biochemical signals (such as transforming growth factor-β; TGF-β).[3,7] Previous studies have shown the effects of TGF-β[3,7,18,19] and the magnitude of shear flow[7] on EndMT; however, the interplay of these stimuli on EndMT and the role of mesenchymally transformed cells in disease progression or tissue regeneration is still not well defined.

Understanding the role of parameters in a physiological environment is more cost effective in microfluidic devices than in animals. Microfluidic devices allow for control of various shear stress magnitudes and direct biochemical factors exposure. Microfluidic devices integrate perfused recirculating cell culture

[a]*Department of Biomedical Engineering, Binghamton University, PO Box 6000, Binghamton, NY 13902, USA. E-mail: gmahler@binghamton.edu*

[b]*Department of Mechanical Engineering, Binghamton University, PO Box 6000, Binghamton, NY 13902, USA*

† Electronic supplementary information (ESI) available. See DOI: 10.1039/c6ra16607e

‡ Currently at the Department of Mechanical Engineering, Colorado State University, Fort Collins, CO 80523, USA.

media leading to close approximation of physiologic fluid to tissue ratio compared to standard *in vitro* static cultures. The most commonly fabricated *in vitro* culture devices such as those fabricated from polydimethylsiloxane (PDMS) allow for controlled structural design of flow channels and three-dimensional (3D) ECM chambers. These 3D ECM chamber incorporated devices usually feature isolated cell lines or multiple cell types seeded on the 3D preserved tissue structure allowing for cell invasion studies.[8–11]

Recently, microfluidic *in vitro* models have been used to investigate the role of biomechanical factors on the endothelium in a 3D tumor-matrix microenvironment.[9,11] Shear stress pattern and magnitudes have been shown to regulate endothelial cell phenotypes, and influence cell–cell junctions and cell–matrix interactions.[7,11–14] In animal studies, it has been found that endothelial cells experience altered hemodynamic forces such as low fluid shear stresses at disease-prone microvasculature regions.[15] In contrast, in disease-protected regions, cells are exposed to relatively higher shear stress.[16] However, the role of fluid shear stress magnitudes on human endothelial cell invasion, leading to transformed mesenchymal cell phenotype that remodel the ECM, is unknown.

Microfluidic devices have been used to show that biochemical factors such as TGF-β induce EndMT, cell invasion and increase mesenchymal marker expression in porcine aortic valve endothelial cells.[7] However, TGF-β-driven activation of human vascular endothelial cell response to fluid shear stress on EndMT has not been fully investigated. On the cellular level, TGF-β plays a pivotal role in cellular signaling pathways that control normal homeostasis and regulate pathological processes.[3,4,7,9,10] In normal homeostasis, TGF-β induces endothelial cells to undergo EndMT and regulate cellular behavior, including cell proliferation, differentiation, and ECM remodeling.[5,17] In pathological processes, TGF-β1, one of the isoforms of TGF-β, influences the disruption of normal tissue homeostasis through autocrine and paracrine signalling[1,20–22] and induces EndMT. These processes can be investigated using *in vitro* microfluidic devices that allow for precise control over the tissue microenvironment at physiologically relevant length and time scales, and require much less of the reagent than macroscale reactors.[9,23,24]

In this study, a microfluidic device with an incorporated 3D ECM architecture was developed to investigate the interplay between steady shear stress rates and TGF-β treatment on EndMT. The 3D ECM maintains a physiological tissue microenvironment that enables the investigation of cell invasion into the surrounding tissue and the role of mesenchymal transformed phenotype in ECM remodeling.[8–11] Additionally, this microscale device integrates perfused recirculating cell culture media leading to close approximation of physiological fluid shear stress and allowing for metabolite exposure, both features that are not available in standard static *in vitro* cell cultures. The results from this investigation can lead to more accurate, directed therapeutic developments and a better understanding of the cellular processes involved in vascular or valvular disease progression.

Materials and methods

Three-dimensional microfluidic device design and fabrication

The microfluidic device used in this study is comprised of three parts: a bottom 25 mm × 75 mm glass slide substrate (VWR® International, Radnor, PA), a middle PDMS layer with a 3 mm height and 5 mm diameter cylindrical chamber at the center, and

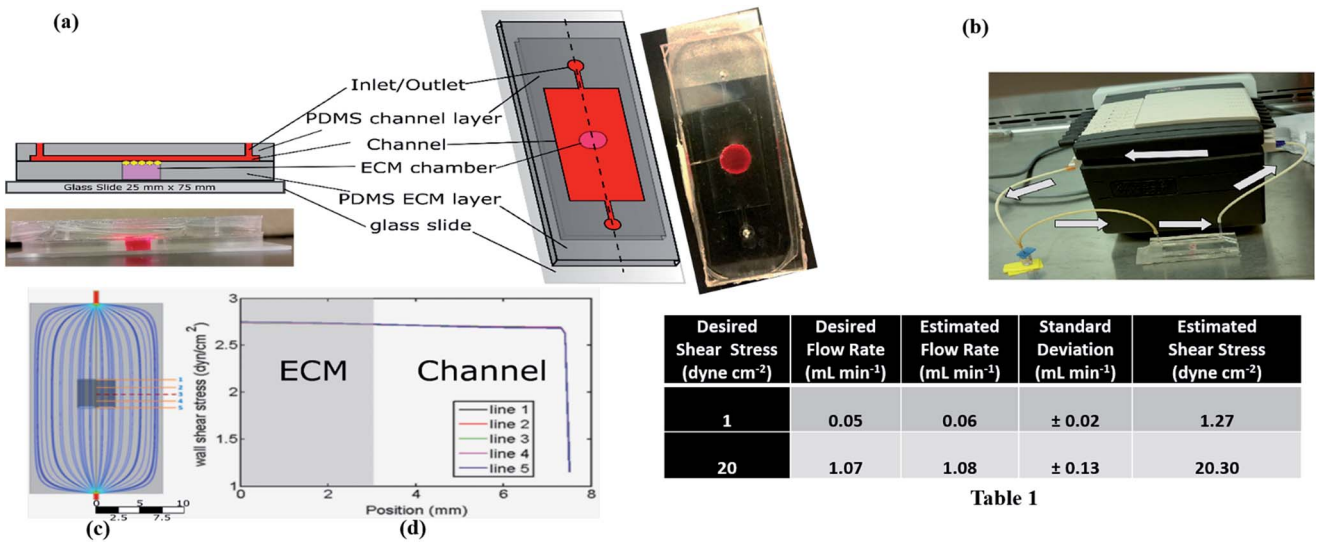

Desired Shear Stress (dyne cm^{-2})	Desired Flow Rate (mL min^{-1})	Estimated Flow Rate (mL min^{-1})	Standard Deviation (mL min^{-1})	Estimated Shear Stress (dyne cm^{-2})
1	0.05	0.06	± 0.02	1.27
20	1.07	1.08	± 0.13	20.30

Table 1

Fig. 1 (a) The microfluidic device is composed of three parts: a glass slide substrate, a middle polydimethylsiloxane (PDMS) layer with a cylindrical chamber at the center, and a top PDMS microchannel with an inlet and an outlet. Human umbilical vein endothelial cells (HUVECs) were seeded on a three-dimensional (3D) extracellular matrix (ECM) collagen gel crosslinked in the chamber. (b) Real-life photo of the peristaltic pump and device set up for applying constant flow on the cells. The reservoir containing culture medium acts as a pulse dampener. (c and d) Computational fluid dynamics (CFD) simulation of flow in the microchannel. (c) Laminar flow streamlines (shown in blue) at a flow rate of 0.05 or 1.07 mL min^{-1}. Lines 1 through 5 represent positions of five different streamlines on the dark gray region, which corresponds to the location of collagen gel where the endothelial cells were seeded. (d) Plot of shear stress at the five different streamlines on the dark gray region. The flow shear stress is nearly constant in the dark gray region. Scale bar = 10 mm. Table 1. Particle tracking velocimetry (PTV) characterization of the shear flow inside microfluidic device.

a top PDMS piece engraved with a rectangular 15 mm wide × 30 mm long × 50 μm deep microchannel with an inlet and an outlet (Fig. 1(a)). The cylindrical chamber houses the collagen gel, which serves as an ECM for the endothelial cells. The microchannel geometry was designed in Inkscape version 0.91 and printed on Mylar photolithography masks (Infinite Graphics Inc., Minneapolis, MN) for soft lithography fabrication.

Fabrication consisted of three steps: photolithography, PDMS replica molding and plasma bonding. First, a silicon wafer mold was created using standard processing protocols. Briefly, a silicon wafer substrate was first cleaned with Nano-Strip® (KMG Chemicals, Inc., Tuscaloosa, AL) solution for 10 minutes to remove any contaminants on its surface. SU-8 2050 negative photoresist (MicroChem Corp., Newton, MA) was then spun onto the wafer for a 50 μm thickness. After a pre-exposure bake, the photoresist was exposed at 360 nm wavelength with an applied intensity of 45 mW cm^{-2} for 6.5 seconds (Suss Microtec MJB4 mask aligner, Garching bei München, Germany) before post-exposure bake and SU-8 structure mold development (SU-8 developer; MicroChem Corp., Newton, MA). The PDMS piece containing the microchannel structure was created by casting PDMS (9 : 1 monomer : cross-linker; Sylgard 184; Dow Corning, Midland, MI) on top of the SU-8 wafer mold. For the ECM chamber-containing PDMS layer, PDMS (9 : 1 monomer : cross-linker; Sylgard 184; Dow Corning, Midland, MI) was casted onto a rectangular aluminium metal mold of 15 mm width × 30 mm length × 3 mm height. After PDMS has crosslinked it was gently peeled off the aluminium mold and a 5 mm diameter hole was created in the PDMS with a Mayhew PRO hollow puncher (Mayhew Steel Products Inc., Turners Fall, MA). This PDMS layer was exposed to oxygen plasma (Herrick Plasma, Ithaca, NY) for 40 seconds at room temperature and permanently bonded to the glass slide substrate. The device assembly was completed when the rectangle PDMS microchannel piece was surface-activated by oxygen plasma (40 second exposure) and permanently sealed against to the PDMS layer containing the 5 mm ECM chamber. After fabrication, the completed device was sterilized in the autoclave before collagen solution was injected and cells were seeded.

A closed-loop media recirculating system was used to create physiologically relevant steady shear low and high flow rates (0.05 and 1.07 mL min^{-1}, respectively) inside the microfluidic device. The inlet and outlet of the microchannel was each joined to flexible tubing (Cole-Parmer Instrument Company, Vernon Hills, IL) connected to a reservoir (Stripwell™, Costar®, Corning Incorporated, Corning, NY) that houses the media. The media in the flexible tubing was perfused into the microchannel by a Watson-Marlow 250S peristaltic pump (Watson-Marlow Pumps Group, Paramus, NJ) operating at a constant motor speed for 48 hours (Fig. 1(b)). The microfluidic system (pump, reservoir, and device) was placed in a 37 °C humidified incubator with 5% CO_2 during cell culture.

Computational fluid dynamics (CFD) simulation of shear flow in the device

The *in vitro* experiments require that the flowing culture medium exerts a uniform shear stress of 1 to 20 dynes per cm^2 on the endothelial cells seeded atop the collagen layer located at the center of the microfluidic device. We thus conducted a computational study of the fluid flow fields under different chamber designs to test this requirement and to ensure that no flow separation in any region of the microfluidic device is created. Properties of water at 37 °C are used to represent the culture medium. All of the computational fluid dynamics models were implemented in the commercial software package ANSYS FLUENT 14.0 (ANSYS Inc., Canonsburg, PA). The boundary conditions include an imposed inlet volumetric flow rate and no-slip boundary conditions on all solid walls of the microchannel. The gel layer is assumed to impermeable with a no-slip boundary condition. Alexiou and Kapellos reported that negligible flow flux can be expected in a poroelastic gel with a pressure-driven flow over its surface if the characteristic Darcy number is less than 10^{-4}.[25] A recent experimental measurement by Moreno-Arotzena *et al.* showed that type I collagen at a final concentration of 2 mg mL^{-1} (similar to our 1.5 mg mL^{-1}) has a Darcy's permeability of $K = 1 \times 10^{-12}$ m^2.[26] With a gel chamber height of $H = 3$ mm, we have a Darcy number of $Da = K/H^2 \approx 1.11 \times 10^{-7}$, which justifies our impermeable gel assumption.

The length of the inlet channel is set to be 2000 μm to ensure that the flow becomes fully-developed at the testing region. The magnitude and uniformity of the shear stress imposed on the endothelial cells depending on microchannel dimensions and geometry. It is found that a flow channel with a rectangular geometry is the best choice to satisfy the requirements of the experimental conditions because this geometry leads to the best shear stress uniformity in the test region where endothelial cells are seeded. Fig. 1(c) illustrates the microchannel with flow streamlines (blue lines). The ECM chamber is depicted in the center of the microchannel where the wall shear stress profile at 5 different cross sections (orange lines labelled 1 to 5) are characterized. Fig. 1(d) shows that an ECM chamber placed at the center of the microchannel is exposed to nearly uniform level of shear stress.

Flow characterization of microfluidic device

To validate the fabricated microfluidic device in imposing the desired level of shear stress on the HUVECs, we conducted particle tracking velocimetry (PTV) flow measurements and compared the measured mean flow velocities with theoretical values. The theoretical volumetric flow rates for 1 and 20 dynes per cm^2 steady shear stresses on the cells inside the ECM chamber are 0.05 and 1.07 mL min^{-1}, respectively. Water containing 1 μm diameter fluorescent beads in low volume fraction (0.01% of microbeads in water v/v) were injected into the microchannel in steady, continuous flows. Videos of the tracers in flow were captured and analyzed with ImageJ 1.48v (National Institutes of Health, USA)[27] manual tracking plugin. The trajectories of over 50 fluorescent tracers were calculated to determine their average velocities. Using the mean velocity of the beads, flow rate and shear stress are calculated based on microchannel geometry. A video of the fluorescent microbeads flowing at the bottom wall of microchannel over collagen gel can be found in the ESI Video I.†

Three-dimensional collagen gel constructs

Before collagen gel solution introduction, all devices and flow setups were autoclaved for sterilization. Collagen gel solution was constructed to a final concentration of 1.5 mg mL^{-1} by mixing ice-cold 3× Dulbecco's Modified Eagle's Medium (DMEM; Life Technologies, Grand Island, NY), sterile 18 MΩ water, 10% fetal bovine serum (FBS; Life Technologies), 0.1 M NaOH, and rat tail collagen type I (BD© Biosciences). For static collagen gel experiments, 300 μL of the solution was plated into each well of the 4-well tissue culture plate (1.9 cm^2 growth area; Thermo Scientific Nunc). After 1 hour of incubation at 37 °C and 5% CO_2, cells were seeded onto the gels in each well. For microfluidic high shear flow experiments (20 dynes per cm^2), PDMS chamber was treated with poly-D-lysine hydrobromide (PDL; 50 μg mL^{-1} Sigma-Aldrich, St. Louis, MO) was introduced to the chamber and incubated for 1 hour at 37 °C to enhance collagen gel adhesion. The chamber was then aspirated and washed with 1× PBS (Phosphate-Buffer Solution, OmniPur®, Baltimore, MD) to render the chamber surface. Then Cell-TAK (Corning® Life Technologies) at a concentration of 50 μg mL^{-1} in 1× PBS was added to the chamber and incubated for 20 minutes at 37 °C. The chamber was again aspirated and washed with 1× PBS before forming collagen gels inside. For microfluidic low and high shear stress experiments, 200 μL of the pre-collagen solution was injected into the side of the PDMS chamber with a 1 mL syringe (Tuberculin Slip Tip Syringe, Becton, Dickson and Company; BD, Franklin Lakes, NJ) and a 23 gauge 1-inch needle (23G1 PrecisionGlide™ needle, Becton, Dickson and Company; BD, Franklin Lakes, NJ). Immediately after pre-gel solution injection the needle hole was patched with silicone glue (100% silicone, General Electric, Fairfield, CT) and incubated for 30 minutes at room temperature then additional 30 minutes of incubation at 37 °C and 5% CO_2 before seeding the cells.

Collagen gel mechanical measurement

We measured the collagen gel mechanical stiffness to provide a comparison to native and pathological tissue measurements. A rheometer (AR 1000, TA Instruments, New Castle, DE) was used to perform the measurements. For 1.5 mg mL^{-1} collagen samples the elastic modulus was determined to be 2.45 ± 0.45 kPa.[28] Depending on location, composition and type of tissue *in vivo* conditions exhibit a gradient of stiffnesses (*e.g.* elastic modulus of brain tissue ranges from 0.1–1 kPa and muscles ranges from 8–17 kPa).[29,30] Pathological tissues, such as tumors range from 6.66 ± 2.66 to 39.99 ± 5.33 kPa.[31] The stiffness (elastic modulus) of blood vessels ranges from 0.2–4.0 kPa.[32,33] Our 1.5 mg mL^{-1} collagen gel stiffness of 2.45 ± 0.45 kPa falls within this range.

Cell culture

Human umbilical vein endothelial cells (HUVECs, Lonza) were cultured at 37 °C and 5% CO_2 in endothelial cell basal medium-2 (EBM-2) supplemented with the EGM-2 reagents: 2% fetal bovine serum (FBS), 0.1% recombinant human epidermal growth factor recombinant (rheGF), 0.1% vascular endothelial growth factor (VEGF), 0.1% ascorbic acid, 0.1% recombinant long insulin like growth factor (R3-IGF-1), 0.1% gentamicin sulfate amphotericin-B (GA-1000), 0.4% recombinant human fibroblast growth factor-B (rhGF-B) and 0.04% hydrocortisone (Lonza, percentages by volume). Cells between passages 2 and 9 were used for all the experiments. Cells were passaged every 4–5 days using 0.25% trypsin–EDTA for cell detachment, followed by trypsin neutralization solution (TNS; Lonza) treatment. Cells were then pelleted by centrifugation at 220 relative centrifugal force (RCF) for 5 minutes and cell count was performed using a hemocytometer with trypan-blue exclusion. For routine culture, HUVECs were seeded at a density of 10 000 cells per cm^2. For static collagen gel experiments, cells were seeded at 2×10^5 cells per cm^2 onto the collagen gels in 4-well tissue culture plates. HUVECs suspended in 300 μL culture medium were seeded onto collagen gel in each well and incubated at 37 °C and 5% CO_2 for 4 hours. For dynamic experiments, HUVECs (5×10^5 cells per cm^2) suspended in 60 μL culture medium were injected into the microfluidic device. The cells were allowed to attach onto the collagen gel for 4 hours in the incubator at 37 °C and 5% CO_2. Shear stress values of 1 and 20 dynes per cm^2 were then applied for 48 hours in the experiments.

Biochemical stimulation with TGF-β1

To study the role of altered biochemical stimulation on EndMT, HUVECs attached to collagen gels under static and flow conditions were treated with TGF-β1 (Gemini Bio-Products, West Sacramento, CA) after HUVEC incubation for 4 hours at 37 °C and 5% CO_2. For static experiments, EGM™-2 culture medium or the EGM™-2 culture medium + 10 ng mL^{-1} TGF-β1 was added to each well. For dynamic experiments, EGM™-2 culture medium or the EGM™-2 culture medium + 10 ng mL^{-1} TGF-β1 was added to each reservoir during medium recirculation.

Real time-quantitative polymer chain reaction (RT-qPCR)

After 48 hours, gels were removed from 4-well plates under static conditions or from the device under shear conditions. HUVEC RNAs were extracted and purified from each collagen gel using RNeasy® Mini Kit (Qiagen, Valencia, CA). Reverse transcriptase was then carried out to synthesize the deoxyribonucleic acid (DNA) using iScript™ cDNA Synthesis Kit (BioRad, Hercules, CA). RT-qPCR was then performed using Mini Opticon Real-Time PCR System (BioRad, Hercules, CA). The genes examined encode for endothelial cell–cell junction (VE-cadherin; CDH5), mesenchymal transformation (α-SMA, ACTA2; Snail), inflammatory cytokines (vascular cell adhesion molecule 1 (VCAM-1)) and intercellular cell adhesion molecule 1 (ICAM-1),[34] and fibrosis collagen type I alpha 2 (COL1A2) markers. Gene expression values were quantified using the DDC_t method with glyceraldehydes-3-phosphate dehydrogenase (GAPDH) as a housekeeping gene. Primers used for RT-qPCR are listed in Table 1 of the ESI.†

Immunocytochemistry staining of cell–cell gap junctions, alpha-smooth muscle actin and collagen type I production

After 48 hours under static or shear conditions, HUVECs on 3D collagen gels were fixed and stained for tight junction and α-SMA or collagen type I production and α-SMA. Under static and shear conditions, HUVECs on 3D collagen gels were washed with PBS, fixed *in situ* with 4% paraformaldehyde (Sigma-Aldrich, St. Louis, MO), and incubated overnight at 4 °C. For static conditions, immunocytochemical staining was performed on the gels within the 4-well plates. For shear conditions, the microfluidic device was gently pulled apart and the gel was transferred from the PDMS chamber with a tweezer into a 96 well cell culture plate (Costar®, Corning Incorporated, Corning, NY). Then, cell membranes were permeabilized with 0.2% Triton X-100 (Sigma-Aldrich, St. Louis, MO) in PBS. After, the cells were washed three times with PBS. A bovine serum albumin (BSA, Rockland, Inc., Gilbertsville, PA) solution was added next (1% BSA in PBS, w/v) and left overnight at 4 °C. After 24 hours, BSA was removed, primary antibodies were added onto the gels and allowed to incubate overnight at 4 °C. For tight junction and α-SMA studies, VE-Cadherin (1 : 200 v/v, rabbit anti-human; Cell Signaling Technology, Inc., Danvers, MA), and α-SMA, (1 : 100 v/v, mouse anti-human, Spring Bioscience, Inc., Pleasanton, CA), were added. For collagen type I production and α-SMA studies, anti-collagen type I antibody (1 : 100 v/v, mouse monoclonal to collagen I, Abcam, Cambridge, UK) and α-SMA, (1 : 100 v/v, mouse anti-human, Spring Bioscience, Inc., Pleasanton, CA), were added. After incubation, cells were washed and 1 : 100 dilutions of secondary antibodies (Alexa Fluor® 568 and Alexa Fluor® 488, Invitrogen, Grand Island, NY) were added for 2 hours in the dark at room temperature. After that, the cells were rinsed once more and a 1 : 1000 dilution of 5 mM DRAQ 5 (Thermo Fisher Scientific, Inc., Rockford, IL) was added. Finally, the cells were again incubated for 30 minutes at room temperature and then rinsed with 18 MΩ water. For static and shear conditions, fixed and stained gels were sandwiched between a glass slide and coverslip (24 × 40 mm micro cover glass no. 1 SUPERSLIP, VWR® International, Radnor, PA) and fluorescent images were obtained using a Leica TCS SP5 confocal imaging system with a 63× water-immersion objective. Five confocal images from each condition were captured and analyzed using a MATLAB (Mathworks, Natick, MA) custom written code to quantify fluorescent intensity of α-SMA protein expression.

Cellular morphology and filamentous (F-actin) cytoskeletal organization analysis

After 48 hours of exposure to static conditions, low, or high shear stress, HUVECs were fixed *in situ* with 4% paraformaldehyde overnight at 4 °C. Then the cells were stained with AlexFluor-488-phalloidin fluorescent dye at a 5 : 200 dilution and incubated for 20 minutes at room temperature on a rocker (Invitrogen Inc., Eugene, OR). Phalloidin staining was used to investigate the filamentous (F-actin) cytoskeleton alignment altered by fluid flow. Finally, the cells were rinsed three times with 1× PBS. For DNA staining, a 1 : 1000 dilution of 5 mM DRAQ 5 (Thermo Fisher Scientific, Inc., Rockford, IL) was added into the gels and incubated for 30 minutes at room temperature. Following incubation the gels were rinsed with 18 MΩ water. Five representative confocal images were taken using a Leica confocal TCS SP5 confocal imaging system with a 63× water-immersion objective. These images were analyzed with ImageJ to determine the cell shape index (SI) and orientation angle (OA) of HUVECs seeded on 3D collagen gels under static and shear conditions. SI is a non-dimensional parameter that quantifies cell elongation on a scale of 0 to 1, with 0 being a flat line and 1 a perfect circle. The cell shape index (SI) is calculated from the following equation: $SI = (4\pi \times \text{cell area})/(\text{cell perimeter})^2$.[23] For F-actin angle measurements degrees of deviation from flow were depicted for OA to be between 0 to 90 degrees, with OA = 0 degree being the streamwise direction and OA = 90 degrees being perpendicular to the flow (OA = 45 degrees is randomly oriented). Scale was constant throughout collection of data. The SI and OA measurements were determined for 50 cells.

VE-cadherin junctional gap width quantification

Junctional gap width measurements were performed with ImageJ. Using fluorescently stained confocal images of VE-cadherin, a perpendicular line was drawn across gap junctions per cell and the distance was recorded with respect to intensity profiles using ImageJ. Data was graphed to represent the gap widths obtained under no, low, and high shear stresses with and without TGF-β1 treatment.

Invasion assay

After 48 hours, cell invasion assays were performed on all collagen gel samples under static or shear conditions with and without TGFβ-1 treatment. HUVECs invasion into the collagen gels were measured by counting the number of transformed cells invading to a depth of 60 μm in four different fields of view in each well observed under bright field microscopy. The average number of invaded HUVECs were correlated with TGFβ-1 and shear stress exposure.

Statistics

All data were analyzed using a one-way or two-way ANOVA with a Tukey's *post hoc* testing $n \geq 3$, $P < 0.05$ using Graphpad Prism version 5 for windows (GraphPad Software, San Diego, CA).

Experimental results and discussion

PTV measurements confirmed desirable flow characterization

Previous studies have established that hemodynamic forces as a principle factor in endothelial barrier function.[35] Normal endothelial cell function occurs at the arterial shear stress level (>15 dynes per cm^2), while low shear stress (<4 dynes per cm^2) are found in pathologies such as atherosclerotic plaques[35] and near tumors.[36] Experiments were designed to apply hemodynamic forces on HUVECs at low (1 dyne per cm^2) and high (20 dynes per cm^2) fluidic shear stress levels. Table 1 compares the desired and measured flow rates within the microchannel near

the ECM. These results of measured flow rates were in close approximation to the desired flow rate values with an overall low standard deviation. Additionally, these flow rates are in agreement with the values obtained from the CFD simulations.

Altered shear flow effect on cellular morphology and F-actin cytoskeletal organization

Steady shear flow was applied for 48 hours to HUVECs seeded on 3D collagen gels deposited within the ECM chamber in the microfluidic device. Immunofluorescence stained images of HUVEC F-actin alignment under static, low and high shear stress conditions are shown in Fig. 2(a–c). We examined characteristics of the HUVECs by analyzing cell-shape and F-actin cytoskeletal organization, and observed that shear flow altered cell morphology in contrast to the static control results.

For cell shape analysis, SI is 1.0 when a cell's nuclei is perfectly circular and decreases when a cell's nuclei is stretched. Shown in Fig. 2(d), the average SI of HUVECs under static control conditions is 0.85 ± 0.09. For HUVEC exposed to steady shear stress, SI reduced to 0.78 ± 0.25 and 0.81 ± 0.15 for low and high stress magnitudes, respectively. Statistically, HUVECs under static, low, or high shear flow conditions showed no significant difference in cell circularity. Previous studies have showed when endothelial cells were seeded on 2D fibronectin treated surfaces and on coverslip in a parallel-plate flow chamber cells elongated after exposure to shear stress of 12.08 dynes per cm^2 for 6 hours and 15 dynes per cm^2 for 24 hours with an SI of 0.61.[23,37] In this study, we seeded human endothelial cells on 3D collagen similar to the ECM of the arterial wall.[38]

There was significant difference in the F-actin alignment in HUVECs under high shear flow condition compared to static control. The average OA of HUVECs F-actin cytoskeletal organization was 22.07 degrees under high shear stress compared to 56.57 degrees for low and 57.84 degrees for static conditions (shown in Fig. 2(e)). The results demonstrate that HUVECs grown on 3D gels and exposed to high shear were aligned in the streamwise direction. For static conditions and low shear exposed cells were approximately random oriented. For static conditions, these findings are consistent with other studies that have demonstrated that shear stress mediates endothelial cell F-actin alignment *in vitro*.[23,37,39] Galbraith *et al.* demonstrated that endothelial cells exposed to high shear stress (15.2 ± 0.1 dynes per cm^2) respond and rearrange F-actin cytoskeletal organization. Our results on endothelial cell morphological changes are comparable with *in vivo* studies that show cells in straight, nonbranched vessel areas exposed to low shear stress are round in shape, with random and short actin filaments located at cell periphery.[40] While high shear stress promotes an increase in alignment of actin stress fibers in the direction of flow.[41] This endothelial cell morphology modification in response to shear is critical for the maintenance of endothelial cellular functions such as proliferation.[42]

Shear stress magnitude and TGF-β1 regulate VE-cadherin, inflammatory, EndMT and collagen production gene expression levels in HUVEC

For RT-qPCR characterization, we examined endothelial marker VE-cadherin (CDH5), inflammatory cytokines (VCAM-1, ICAM-1), pro-EndMT markers (ACTA2, Snail), and fibrosis marker (COL1A2) gene expression in HUVEC under static conditions, low or high steady shear flow, with and without exposure to TGF-β1 (as shown in Fig. 3). Gene expression for all conditions were compared to static control condition. VE-cadherin/CDH5

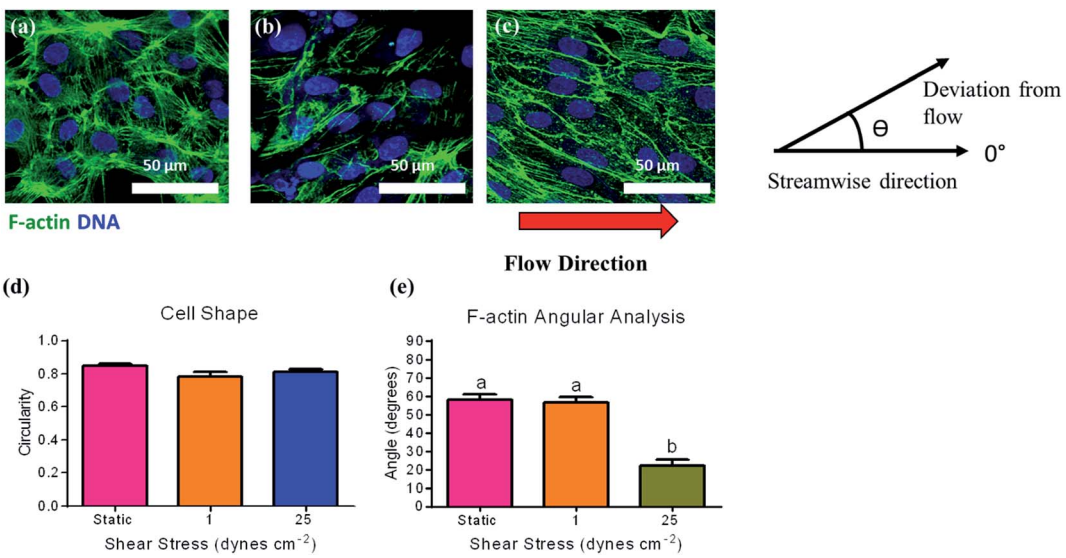

Fig. 2 Immunostainings of filamentous (F-actin) cytoskeletal organization. Human umbilical vein endothelial cells (HUVECs) were exposed for 48 hours to (a) static conditions, fluid shear stress of (b) low at 1 or (c) high at 20 dynes per cm^2. Cells were counterstained for F-actin (green) and deoxyribonucleic acid (DNA; blue), arrows indicate the direction of fluid flow. Scale bar = 50 μm. Cell shape and alignment were quantified by (d) cell circularity and (e) F-actin alignment. Error bars show SEM, n = at least 50 cells from representative confocal images. Bars that don't share any letters are significantly different according to a one-way ANOVA with Tukey's *post hoc* testing ($P < 0.05$).

gene expression remained statistically the same in sheared and static conditions, except for low shear with TGF-β1 (upregulated by 1.45 ± 1.42 fold), as shown in Fig. 3(a). These results state the presence of uniform endothelial monolayer when cells are exposed to all conditions with and without TGF-β1.

Gene expression of inflammatory encoded genes VCAM-1 and ICAM-1 was upregulated by 2.12 ± 0.28 fold and 3.93 ± 1.33 fold, respectively in HUVECs exposed to TGF-β1 under low shear flow, shown in Fig. 3(b and c). VCAM-1 expression was downregulated by 0.26 ± 0.09 fold and ICAM-1 upregulated by 2.97 ± 1.1 fold for high shear flow with TGF-β1 exposure. Inflammation gene expression are consistent with endothelial cells exposed to low shear stress in a parallel-plate or cone-and-plate chamber showing the presence of VCAM-1 and ICAM-1.[43,44] Increased expressions of ICAM-1 and VCAM-1 in endothelial cells has been observed *in vivo* at atherosclerosis prone areas.[45,46]

ACTA2 was found to be significantly upregulated for cultures without TGF-β1 treatment, 10.24 ± 4.63 fold and by 25.31 ± 4.90 fold under low and high shear conditions, respectively. With TGF-β1 exposure, ACTA2 gene was upregulated by 1.12 ± 0.35 fold, 45.81 ± 11.78 fold, and 7.67 ± 3.90 fold for static conditions, low and high shear stress, respectively, as shown in Fig. 3(d). These results demonstrate that α-SMA encoded gene is highly expressed in HUVECs cultured with low shear flow and TGF-β1 exposure, while decreased under high shear and TGF-β1 treatment. Snail, a pro-EndMT gene that represses the expression of the adhesion molecule E-cadherin, was upregulated by 17.79 ± 2.46 fold for high shear flow compared to static control, as shown in Fig. 3(e). This result agrees with a study performed by Lawler *et al.*, which showed that shear stress resulted in E-cadherin internalization.[47] These gene expression results suggest that HUVEC undergo EndMT when exposed to low shear stress and/or TGF-β1. These data also depicts that TGF-β1 and high shear stress exposure down regulates EndMT-associated gene expression (ACTA2) in HUVECs.

Lastly, fibrosis marker COL1A2 was upregulated only in static conditions with and without TGF-β1 treatment. COL1A2 was downregulated by 0.18 ± 0.11 fold and 0.583 ± 0.6 fold for low and high shear flow, respectively, as shown in Fig. 3(f). With TGF-β1 exposure, COL1A2 expression was downregulated by 0.40 ± 0.05 fold and 0.19 ± 0.08 fold under low and high shear stresses, respectively. These results show that under static conditions with and without TGFβ-1, cells are able to produce the most collagen type 1, similar to fibrotic conditions. Contrary to static conditions, under shear stress (low and high flow), cells reduce the production of collagen type I. These results suggest that collagen production in transformed cells is high under static with and without TGF-β1 conditions.

Shear flow and TGF-β1 increased endothelial cell–cell gap junction width, α-SMA protein expression, HUVEC invasion and collagen type I production

Confocal images of HUVECs captured 48 hours after exposure to static condition, low or high shear stress with and without TGF-β1 treatment demonstrated uniform expression of cell–cell junction marker VE-cadherin throughout all samples, as shown in Fig. 4(a). These findings are similar to *in vivo* conditions where cell–cell junctions are produced on adjacent cells and only form when cells are fully confluent. Continuous staining of VE-cadherin is a physical marker of endothelium function.[48] We further quantified the HUVEC boundaries by examining the cell–cell junction permeability in terms of gap width. It was

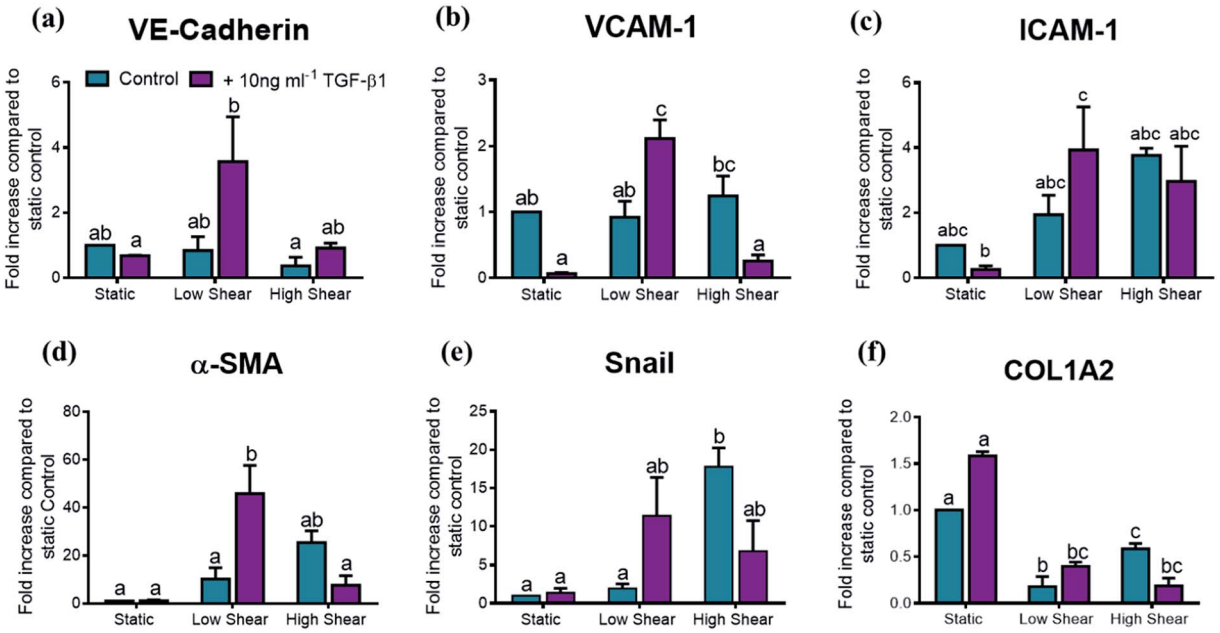

Fig. 3 Gene expression results of (a) vascular endothelial-cadherin (VE-cadherin; CDH5), (b) inflammation encoded genes vascular cell adhesion molecule-1 (VCAM-1) and (c) intercellular adhesion molecule-1 (ICAM-1), and (d) endothelial to mesenchymal transformation (EndMT) markers, actin, alpha 2 (ACTA2) and (e) Snail. Lastly, (f) the fibrosis marker; collagen type 1 alpha 2 chain (COL1A2). Error bars show SEM, $n = 3$ culture wells. Bars that don't share any letters are significantly different according to a two-way ANOVA with Tukey's *post hoc* testing ($P < 0.05$).

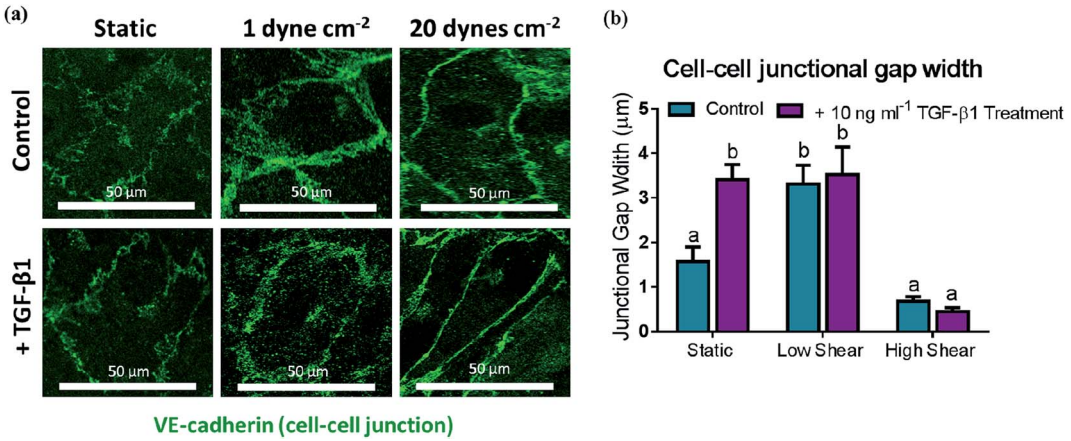

Fig. 4 (a) Vascular endothelial-cadherin (VE-cadherin) junctions (green) of human umbilical vein endothelial cells (HUVECs) exposed to static conditions, fluid shear stress levels of low at 1 or high at 20 dynes per cm^2 with and without transforming growth factor-beta 1 (TGF-β1). Scale bar = 50 μm. (b) Quantification of endothelial cell–cell gap junction width measurement. Error bars show SEM, $n = 30$ gap junctions from 3 confocal images. Bars that don't share any letters are significantly different according to a one-way ANOVA with Tukey's *post hoc* testing ($P < 0.05$).

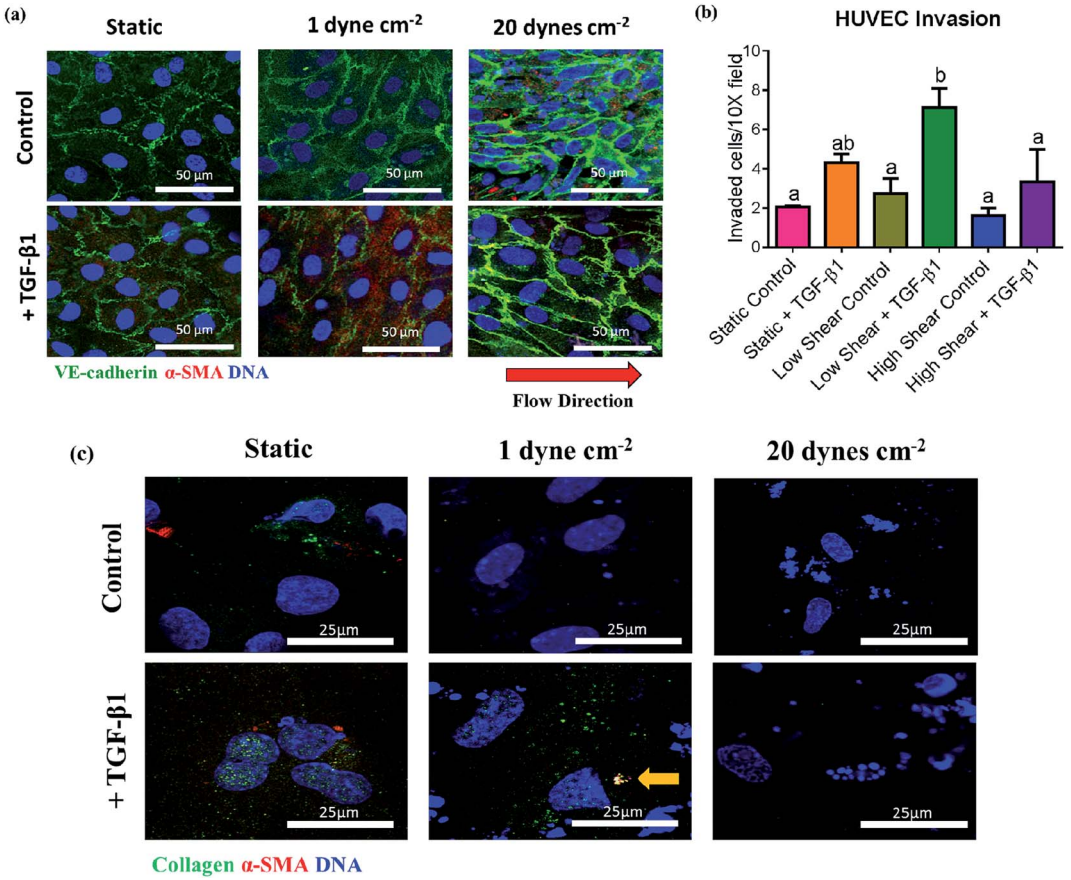

Fig. 5 (a) Human umbilical vein endothelial cells (HUVEC) immunocytochemistry images for alpha-smooth muscle actin (α-SMA; red), vascular endothelial-cadherin (VE-cadherin; green) and cell's DNA (blue) on three-dimensional (3D) collagen gels after 48 hours of exposure to static, static conditions + 10 ng mL^{-1} of transforming growth factors-βeta 1 (TGF-β1), 1 dyne per cm^2 shear flow, 1 dyne per cm^2 shear stress + 10 ng mL^{-1} TGF-β1, 20 dynes per cm^2 shear flow, and 20 dynes per cm^2 shear stress + 10 ng mL^{-1} TGF-β1. Scale bar = 50 μm. (b) HUVEC invasion of cells exposed to static conditions, low (1 dyne per cm^2) or high (20 dyne per cm^2) shear stress with and without TGF-β1. Error bars show SEM, $n = 4$ culture wells. Bars that don't share any letters are significantly different according to a one-way ANOVA with Tukey's *post hoc* testing ($P < 0.05$). (c) HUVEC immunocytochemistry for collagen type I production (green), α-SMA (red), and cell's DNA (blue) on 3D collagen gels after 48 hours in culture. Yellow arrow depicts location of collagen production and α-SMA protein expression in the cell's cytoplasm. Scale bar = 25 μm.

determined that HUVEC exposed to TGF-β1 treatment under static plus TGFβ-1 condition and low shear flow (with and without TGFβ-1) conditions presented the widest gap junctions.

Quantitative junctional gap width data is present in Fig. 4(b). These results demonstrate that high shear stress (with and without TGF-β1) reduced junctional gap width, while low shear flow (with and without TGF-β1) and static with TGFβ-1 conditions increased the gap width between the cells. Under static conditions with TGF-β1 and low shear flow (with and without TGF-β1), the endothelial cell–cell adhesions are more permeable as evidenced by increasing junctional gap width. Tighter junctional gap width observed under high shear stress are most likely related to cell morphology and alignment in the direction of flow.[36] Price *et al.* and Buchanan *et al.* findings are consistent with ours showing that high shear stress increased endothelial monolayer integrity.[36,49]

We further examined characteristics of HUVECs by analyzing protein expression of EndMT marker α-SMA. Confocal images of VE-cadherin and α-SMA stained HUVECs are shown in Fig. 5(a). HUVECs expression of α-SMA was increased under low shear flow with and without TGF-β1 exposure when compared to static control conditions. Intensity profiles of α-SMA marker expression were consistent in HUVECs exposed to all conditions except under high shear stress with and without TGF-β1 treatment (results shown in Fig. 1 of the ESI†). HUVECs exposed to high shear flow with and without TGF-β1 decreased the expression of α-SMA marker by 0.66 ± 0.08 fold and by 0.74 ± 0.6 fold, respectively, when compared to static control condition. These observed α-SMA marker protein expression results suggest that endothelial cells are ready to invade into the 3D collagen gel with the assistance of TGF-β1 under low shear stress condition; however, HUVECs exposed to high shear stress condition reduces α-SMA expression. For HUVEC invasion into the matrix, an average of 7.13 ± 1.93 cells exposed to low shear stress with TGF-β1 treatment invaded, while only 3.36 ± 0.32 cells invaded under the static control condition, as shown in Fig. 5(b). Lastly, to confirm that the mesenchymally transformed phenotype cells produced collagen type I within the ECM, confocal images of collagen production were captured for all conditions, as shown in Fig. 5(c). HUVECs exposed to static and low shear stress conditions with TGF-β1 treatment formed more collagen compared to the static control and high shear stress conditions. Additionally, local to the regions of collagen production, α-SMA protein expression was observed, suggesting that the HUVECs that underwent EndMT transitioned into activated fibroblasts. It has been observed in this study that endothelial cells under the static condition with TGF-β1 treatment transformed into activated fibroblastic-like phenotype cells and produced a reactive ECM that is significantly different from normal ECM, hence remodeling the surrounding tissue.

These findings are similar to the results of Shapero *et al.* showing that TGF-β1 induces EndMT,[50] and to that of Mahler *et al.* where low shear stress promotes EndMT[7] in endothelial cells. A full summary of the data from this study can be found in ESI Table 2.† Our results are unique in that TGFβ1-induced EndMT effect can be inhibited in cells exposed to high shear stress. They also suggest that endothelial cells exposed to shear stress with TGF-β1 promotes cell motility (increased α-SMA expression and invasion into the matrix), causing changes in cellular function. Shear stress conditions are known to play a role in the behavioral changes of endothelial cells[51] and this was also observed in this study.

A step by step process of EndMT based on our results is illustrated in Fig. 6. Initiation with vascular or valvular endothelial cells phenotype form a cell monolayer, express VE-cadherin, and adhere *via* α and β integrin subunits onto the ECM that is comprised of collagen protein (illustrated in Fig. 6(a)). Activated endothelial cells express inflammatory cytokines gene (VCAM-1 or ICAM-1) on the surface, as illustrated in Fig. 6(b). Next the transformed cells (increased junctional gap width, low VE-cadherin, high α-SMA gene and protein expression) have the ability to invade into the ECM, as illustrated in Fig. 6(c). Finally, the EndMT cells which have the

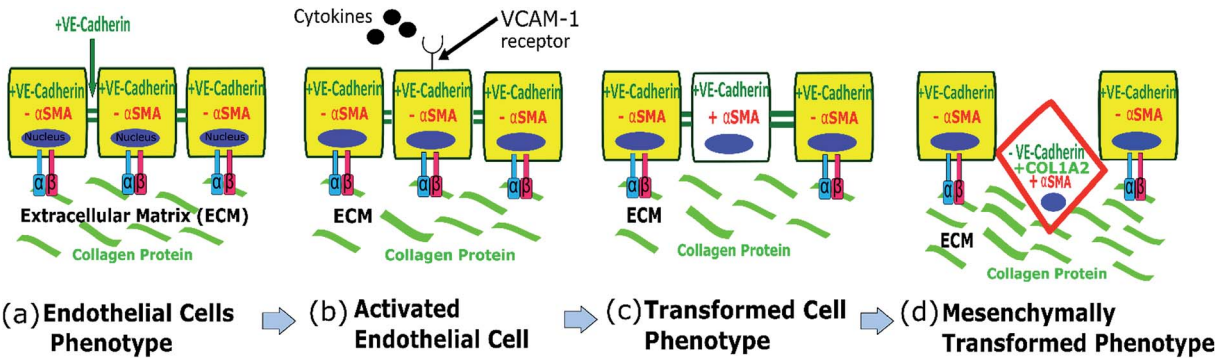

Fig. 6 Illustration of the endothelial to mesenchymal transformation (EndMT) process. (a) Initially, quiescent vascular or valvular endothelial cell form a cell–cell monolayer expressing vascular endothelial-cadherin junctional marker between cells (+VE-cadherin; symbol (=)). These endothelial cells normally adhere *via* alpha and beta (α and β) integrin subunits onto the extracellular matrix (ECM), which is comprised of collagen protein. (b) A single endothelial cell may become activated and express inflammatory receptors on the endothelial cell surface. (c) This cell is then able to acquire mesenchymal-like characteristics, such as alpha-smooth muscle actin (α-SMA) expression and increased junctional permeability (symbol (=)). (d) Lastly, this transformed mesenchymal-like cell is able to invade into the ECM and remodel the tissue by upregulation of the collagen type 1 alpha 2 (COL1A2) gene and increased collagen production. Note: symbols (+) expression and (−) no expression.

potential to differentiate into activated fibroblasts and are involved in remodeling the ECM (highest collagen production protein and gene expression), as illustrated in Fig. 6(d). We hypothesize that the few endothelial cells that underwent EndMT under static conditions are most likely to generate activated fibroblasts, seen with the upregulation of COL1A2 gene and protein expression. These activated fibroblasts are involved in remodeling the ECM and involved in collagen production causing fibrosis. Thus, under static conditions the most activated fibroblasts production was observed, but not the most EndMT (invasion, α-SMA protein and gene expression) process. HUVECs underwent EndMT when exposed to low shear stress with TGF-β1 treatment. HUVECs undergone the EndMT process the least and reduced activated fibroblast formation occurred when exposed to high shear stress and TGF-β1 treatment. This data presented agrees with previous *in vitro* and *in vivo* EndMT studies.[6,50,52–54] A possible explanation for this observation could be due to the oscillatory and low steady shear stress conditions endothelial cells experience in pathologies such as atherosclerosis[51] and cancer.[36] We observed from this study that low shear stress induced EndMT in HUVECs compared to static conditions. These results may help to clarify how EndMT can lead to tissue remodeling involved in vascular or valvular disease progression or tissue homeostasis.

Conclusions

We have developed a microscale *in vitro* platform with an incorporated 3D collagen gel to mimic the microenvironment containing a confluent monolayer of the HUVECs seeded on top of a 3D collagen matrix. This microengineered device can be used to study the role of altered shear stress and growth factor (TGF-β1) on EndMT, a process that is essential during embryonic development and tissue regeneration. In this EndMT study, endothelial cell invasion, altered protein and gene expression were examined. Low magnitude of shear stress showed no significant changes in endothelial morphology, cytoskeletal arrangement, but induced endothelial cell invasion into the 3D collagen gel, and upregulated mesenchymal protein markers and transcription factors. However, high shear stress counteracts TGF-β induced mesenchymal transformation, which is observed in disease-protected regions.

Furthermore, this method can be extended to investigate the role of other shear stress flow patterns (laminar, unsteady, or oscillatory), magnitude range (1, 10, 20 dynes per cm^2) and direction. Likewise, along with fluid shear stress other 3D collagen matrix properties such as porosity, pore size, stiffness and composition are expected to influence endothelial cell invasion, protein and gene expression and can be systematically altered with the microfluidic device.

Until now, the lack of a 3D *in vitro* culture that can control flow conditions and biochemical exposure influencing EndMT has been a major limiting factor in the study of fibrosis and metastasis in physiological conditions. A clear understanding down to the cellular level at the cell–cell and cell–matrix interface will provide new and important insights into the progression of many systemic adult diseases and may provide the basis for new therapeutic approaches.

Acknowledgements

We would like to acknowledge Hoang Ta, who assisted with PDMS device fabrication and wrote the MATLAB code for confocal image analysis. This work was supported by the Research Foundation of the State University of New York at Binghamton, the National Science Foundation CMMI 1436173, and the Clifford D. Clark Graduate Fellowship.

References

1 W. Yu, Z. Liu, S. An, J. Zhao, L. Xiao, Y. Gou, Y. Lin and J. Wang, *Curr. Stem Cell Res. Ther.*, 2014, **9**, 196–204.
2 E. M. Zeisberg, S. E. Potenta, H. Sugimoto, M. Zeisberg and R. Kalluri, *J. Am. Soc. Nephrol.*, 2008, **19**, 2282–2287.
3 E. M. Zeisberg, S. Potenta, L. Xie, M. Zeisberg and R. Kalluri, *Cancer Res.*, 2007, **67**, 10123–10128.
4 D. Medici, E. M. Shore, V. Y. Lounev, F. S. Kaplan, R. Kalluri and B. R. Olsen, *Nat. Med.*, 2010, **16**, 1400–1406.
5 S. B. Jakowlew, *Cancer Metastasis Rev.*, 2006, **25**, 435–457.
6 S. Potenta, E. Zeisberg and R. Kalluri, *Br. J. Cancer*, 2008, **99**, 1375–1379.
7 G. J. Mahler, C. M. Frendl, Q. Cao and J. T. Butcher, *Biotechnol. Bioeng.*, 2014, **111**, 2326–2337.
8 I. K. Zervantonakis, C. R. Kothapalli, S. Chung, R. Sudo and R. D. Kamm, *Biomicrofluidics*, 2011, **5**, 013406.
9 A. D. Wong and P. C. Searson, *Cancer Res.*, 2014, **74**, 4937–4945.
10 W. J. Polacheck, R. Li, S. G. M. Uzel and R. D. Kamm, *Lab Chip*, 2013, **13**, 2252–2267.
11 I. K. Zervantonakis, S. K. Hughes-Alford, J. L. Charest, J. S. Condeelis, F. B. Gertler and R. D. Kamm, *Proc. Natl. Acad. Sci. U. S. A.*, 2012, **109**, 13515–13520.
12 M. B. Esch, D. J. Post, M. L. Shuler and T. Stokol, *Tissue Eng., Part A*, 2011, **17**, 2965–2971.
13 L. K. Chin, J. Q. Yu, Y. Fu, T. Yu, A. Q. Liu and K. Q. Luo, *Lab Chip*, 2011, **11**, 1856–1863.
14 A. D. van der Meer, V. V Orlova, P. ten Dijke, A. van den Berg and C. L. Mummery, *Lab Chip*, 2013, **13**, 3562.
15 P. L. Walpola, A. I. Gotlieb and B. L. Langille, *Am. J. Pathol.*, 1993, **142**, 1392–1400.
16 B. M. Whited and M. N. Rylander, *Biotechnol. Bioeng.*, 2014, **111**, 184–195.
17 G. J. Mahler, E. J. Farrar and J. T. Butcher, *Arterioscler., Thromb., Vasc. Biol.*, 2013, **33**, 121–130.
18 A. F. Ramsdell and R. R. Markwald, *Dev. Biol.*, 1997, **188**, 64–74.
19 G. Paranya, S. Vineberg, E. Dvorin, S. Kaushal, S. J. Roth, E. Rabkin, F. J. Schoen and J. Bischoff, *Am. J. Pathol.*, 2001, **159**, 1335–1343.
20 N. Reymond, B. B. D'Água and A. J. Ridley, *Nat. Rev. Cancer*, 2013, **13**, 858–870.
21 G. Ferrari, B. D. Cook, V. Terushkin, G. Pintucci and P. Mignatti, *J. Cell. Physiol.*, 2009, **219**, 449–458.

22 E. M. Zeisberg, S. Potenta, L. Xie, M. Zeisberg and R. Kalluri, *Cancer Res.*, 2007, **67**, 10123–10128.
23 M. C. Liu, H. C. Shih, J. G. Wu, T. W. Weng, C. Y. Wu, J.-C. Lu and Y. C. Tung, *Lab Chip*, 2013, **13**, 1743–1753.
24 M. A. Guzzardi, F. Vozzi and A. D. Ahluwalia, *Tissue Eng., Part A*, 2009, **15**, 3635–3644.
25 T. S. Alexiou and G. E. Kapellos, *Phys. Fluids*, 2013, **25**, 073605.
26 O. Moreno-Arotzena, J. Meier, C. del Amo and J. García-Aznar, *Materials*, 2015, **8**, 1636–1651.
27 C. A. Schneider, W. S. Rasband and K. W. Eliceiri, *Nat. Methods*, 2012, **9**, 671–675.
28 S. Dahal, PhD thesis, SUNY Binghamton University, 2016.
29 A. J. Engler, S. Sen, H. L. Sweeney and D. E. Discher, *Cell*, 2006, **126**, 677–689.
30 V. L. Cross, Y. Zheng, N. W. Choi, S. S. Verbridge, A. Bryan, L. J. Bonassar, C. Fischbach and A. D. Stroock, *Biomaterials*, 2011, **31**, 8596–8607.
31 P. A. Netti, D. A. Berk, M. A. Swartz, A. J. Grodzinsky and R. K. Jain, *Cancer Res.*, 2000, **60**, 2497–2503.
32 A. Sieminski, R. Hebbel and K. Gooch, *Exp. Cell Res.*, 2004, **297**, 574–584.
33 I. Levental, P. C. Georges and P. A. Janmey, *Soft Matter*, 2007, **2**, 1–9.
34 R. Amaya, A. Pierides and J. M. Tarbell, *PLoS One*, 2015, **10**, 1–18.
35 A. M. Malek and S. L. Alper, *J. Am. Med. Assoc.*, 1999, **282**, 2035–2042.
36 C. F. Buchanan, S. S. Verbridge, P. P. Vlachos and M. N. Rylander, *Cell Adhes. Migr.*, 2014, **8**, 517–524.
37 G. G. Galbraith, R. Skalak and S. Chien, *Cell Motil. Cytoskeleton*, 1998, **40**, 317–330.
38 W. L. K. Chen and C. A. Simmons, *Adv. Drug Delivery Rev.*, 2011, **63**, 269–276.
39 A. M. Malek and S. Izumo, *J. Cell Sci.*, 1996, **109**, 713–726.
40 D. W. Kim, B. L. Langille, M. K. K. Wong and A. I. Gotlieb, *Circ. Res.*, 1989, **64**, 21–31.
41 B. L. Langille, D. Kim and A. I. Gotlieb, *Arterioscler., Thromb., Vasc. Biol.*, 1991, **11**, 1814–1821.
42 Y.-S. J. Li, J. H. Haga and S. Chien, *J. Biomech.*, 2005, **38**, 1949–1971.
43 S. Mohan, N. Mohan, A. J. Valente and E. A. Sprague, *Am. J. Physiol.*, 1999, **276**, C1100–C1107.
44 A. Dardik, L. Chen, J. Frattini, H. Asada, F. Aziz, F. A. Kudo, B. E. Sumpio, N. Haven and W. Haven, *J. Vasc. Surg.*, 2005, **41**, 869–880.
45 J.-J. Chiu and S. Chien, *Physiol. Rev.*, 2011, **91**, 327–387.
46 I. Masseau and D. K. Bowles, *J. Biomed. Sci. Eng.*, 2015, **8**, 789–796.
47 K. Lawler, G. O'Sullivan, A. Long and D. Kenny, *Cancer Sci.*, 2009, **100**, 1082–1087.
48 P. L. Hordijk, E. Anthony, F. P. J. Mul, R. Rientsma, L. C. J. M. Oomen and D. Roos, *J. Cell Sci.*, 1999, **112**, 1915–1923.
49 G. M. Price, K. H. K. Wong, J. G. Truslow, A. D. Leung and J. Tien, *Biomaterials*, 2011, **31**, 6182–6189.
50 J. Hjortnaes, K. Shapero, C. Goettsch, J. D. Hutcheson, J. Keegan, J. Kluin, J. E. Mayer, J. Bischoff and E. Aikawa, *Atherosclerosis*, 2015, **242**, 251–260.
51 J.-J. Chiu and S. Chien, *Physiol. Rev.*, 2011, **91**, 1–106.
52 L. A. van Meeteren and P. Ten Dijke, *Cell Tissue Res.*, 2012, **347**, 177–186.
53 E. M. Zeisberg, O. Tarnavski, M. Zeisberg, A. L. Dorfman, J. R. McMullen, E. Gustafsson, A. Chandraker, X. Yuan, W. T. Pu, A. B. Roberts, E. G. Neilson, M. H. Sayegh, S. Izumo and R. Kalluri, *Nat. Med.*, 2007, **13**, 952–961.
54 R. Kumarswamy, I. Volkmann, V. Jazbutyte, S. Dangwal, D. H. Park and T. Thum, *Arterioscler., Thromb., Vasc. Biol.*, 2012, **32**, 361–369.